

Generic spiral spin liquids

Xu-Ping Yao¹, Jian Qiao Liu^{1,2}, Chun-Jiong Huang¹, Xiaoqun Wang^{3,4}, Gang Chen^{1,5,†}

¹*Department of Physics and HKU-UCAS Joint Institute for Theoretical and Computational Physics at Hong Kong, The University of Hong Kong, Hong Kong, China*

²*International Center for Quantum Materials, School of Physics, Peking University, Beijing 100871, China*

³*School of Physics and Astronomy, Tsung-Dao Lee Institute, Shanghai Jiao Tong University, Shanghai 200240, China*

⁴*Key Laboratory of Artificial Structures and Quantum Control of MOE, Shenyang National Laboratory for Materials Science, Shenyang 110016, China*

⁵*State Key Laboratory of Surface Physics and Department of Physics, Institute of Nanoelectronics and Quantum Computing, Fudan University, Shanghai 200433, China*

Corresponding author. E-mail: †gangchen@hku.hk

Received March 30, 2021; accepted April 14, 2021

Spiral spin liquids are unique classical spin liquids that occur in many frustrated spin systems, but do not comprise a new phase of matter. Owing to extensive classical ground-state degeneracy, the spins in a spiral spin liquid thermally fluctuate cooperatively from a collection of spiral configurations at low temperatures. These spiral propagation wavevectors form a continuous manifold in reciprocal space, i.e., a spiral contour or a spiral surface, that strongly governs the low-temperature thermal fluctuations and magnetic physics. In this paper, the relevant spin models conveying the spiral spin liquid physics are systematically explored and the geometric origin of the spiral manifold is clarified in the model construction. The spiral spin liquids based on the dimension and the codimension of the spiral manifold are further clarified. For each class, the physical properties are studied both generally and for specific examples. The results are relevant to a wide range of frustrated magnets. A survey of materials is given and future experiments are suggested.

Keywords spiral spin liquids, thermal order-by-disorder, Monte Carlo simulation

Contents

1	Introduction
2	Spiral spin liquids: Classification and model construction
2.1	Class with $d_s = 1$ and $d_c = 1$
2.2	Class with $d_s = 1$ and $d_c = 2$
2.3	Examples with $d_c = 0$
3	Finite-temperature behaviors
3.1	Spiral spin liquid regime
3.2	Thermal order-by-disorder
3.3	Specific heat
4	Discussion
4.1	Survey of materials
4.2	Open theoretical questions
4.3	Summary
	Appendix A Lattice geometry and crystal momenta
	Acknowledgements
	References

1 Introduction

1 As an intriguing field in modern correlation physics, frustrated magnetism has attracted much interest in both theoretical and experimental efforts [1]. In general, frustration describes various competing interactions in a system that cannot be satisfied simultaneously. For frustrated spin systems, these interactions refer to exchange interactions between the local magnetic moments. It is expected that strong magnetic frustration could prevent the development of conventional magnetic orders and strongly suppress the ordering temperature. As a result, a wide range of exotic quantum phenomena may emerge, including quantum phases such as quantum spin liquids [2–4] and the spin nematic phase [5]. To understand these novel physics, new concepts represented by the internal gauge structure and fractionalized excitations have been introduced and developed in the past decades [1, 2, 4]. Among these phenomena, quantum fluctuations play a significant role even in the absence of geometric frustration [6].

Surprisingly, when quantum fluctuation is not important or even absent, strong frustration still has the ability to realize rich and interesting physics. One such exam-

*This article can also be found at <http://journal.hep.com.cn/fop/EN/10.1007/s11467-021-1074-9>.
 arXiv: 2011.03007.



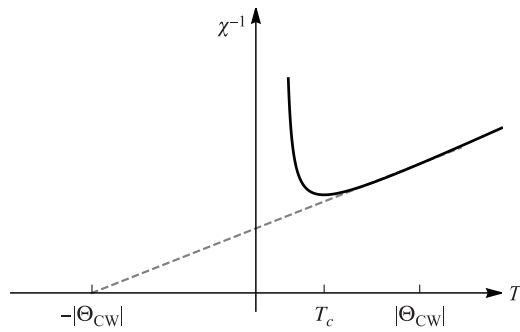


Fig. 1 Magnetic susceptibility of a frustrated antiferromagnet. The classical spin liquid (or cooperative paramagnet) is located in the regime from T_c to $\sim |\Theta_{CW}|$. This would also be the regime for the spiral spin liquid if it is relevant for the underlying system.

ple is the spiral spin liquid that was first proposed for the J_1 – J_2 Heisenberg model on the geometrically unfrustrated diamond lattice [7]. In this spiral spin liquid, the classical ground states are coplanar spin spirals and have macroscopic degeneracy. The propagation vectors of the spiral spin configurations form a continuous manifold dubbed the spiral surface or spiral contour in reciprocal space. At finite temperatures, strong thermal fluctuations on the spiral manifold can stand out from the trivial paramagnetic regime. Hence, there could be a broad spiral spin liquid regime that smoothly connects to the trivial paramagnet in the high-temperature regime, and this spiral spin liquid regime can manifest itself in the spin correlations and thermodynamic properties. Despite being quite interesting, the spiral spin liquid is in the thermal paramagnetic regime and is not really a new state of matter. In Fig. 1, a representative behavior of the magnetic susceptibility of a typical frustrated magnet is depicted in which the spiral spin liquid would be located in the regime from the ordering temperature T_c to the Curie-Weiss temperature $|\Theta_{CW}|$. At very low temperatures, the spiral orderings may develop from so-called thermal order by disorder or from other sub-leading interactions [7, 8]. The external magnetic field could further select a combination of equivalent and coplanar magnetic wavevectors and stabilize non-trivial topological spin structures such as vortices, merons, and skyrmion lattices [9–13].

Recently, the degenerate spiral surface has been confirmed directly by neutron-scattering experiments in a long-promised spin-5/2 diamond-lattice compound MnSc_2S_4 [11, 13] with the single-crystal sample nine years

after the theoretical proposal [7]. This caused a new wave of attention to be paid to the spiral spin liquids, the proximate orders, and the underlying novel physics [12, 14–22]. Although many relevant models and materials have been well studied in past decades, a systematic study for the flourishing family of the spiral spin liquids is still lacking. A recent theoretical work by Attig *et al.* gave a quite complete list of the spin models conveying the spiral manifold [23]. What the authors of Ref. [23] focused on are the spin-fermion correspondence and patterns of spiral manifolds at zero temperature. The resulting behaviors at finite temperatures still remain to be understood. The purpose of this work is to classify the spiral spin liquids, as well as to illustrate the characteristics of their finite-temperature behaviors by constructing the minimal models. The basic idea is to consider the dimensions and codimensions of the spiral manifold (see Table 1). The spin interactions are then designed accordingly and the massively degenerate ground-state manifold effectively manipulated. For both spiral contour and spiral surface cases, a large regime is identified in which spiral spin liquid physics dominates up to a high temperature compared to interactions. The robustness of the spiral spin liquid features is emphasized, which is important for the realization and identification in the realistic materials. Also discussed are the thermal order-by-disorder mechanism [24] and its consequences in three-dimensional systems. It is shown that thermodynamic quantities such as the specific heat would be modified by the induced spiral ordering, and that a distinct temperature dependence is exhibited for spiral manifolds with different dimensions. The scenario of the energy–entropy competition might be more intricate than as demonstrated herein, but is believed to be ubiquitous in real materials [24–26].

The rest of this paper is organized as follows. The spiral spin liquids are reviewed and classified in Section 2. For each class, a general Heisenberg Hamiltonian is constructed to capture the essential physics of a spiral manifold at zero temperature. As quintessences, the square, honeycomb, and AB-stacked multilayered triangular lattices are analyzed in detail. In Section 3, phase diagrams with the temperature and identity of the spiral spin liquid regimes for each case are further established. The difference in the low-temperature specific heat is discussed. Finally, in Section 4, this work concludes with a survey of the existing and potential materials with spiral spin liquid physics, and a discussion about open theoretical questions.

Table 1 Classification of spiral spin liquids. d_s and d_c refer to the dimension and codimension of the degenerate spiral manifold, respectively. “TOBD” refers to the “thermal order-by-disorder” and Θ_{CW} to the Curie-Weiss temperature.

d_s	d_c	TOBD	Stiffness	Low-temperature C_v	Regime for SSL	Model examples
1	1	No	—	$c_1 + c_2T$	$0 \sim \Theta_{CW} $	See Sections 2.1 and 4.1
2	1	Yes	$T^{2/3}$	$c_1 + c_2T^{1/3}$	$T_c \sim \Theta_{CW} $	Diamond lattice J_1 – J_2 model [7]
1	2	Yes	T	$c_1 + c_2T$	$T_c \sim \Theta_{CW} $	See Sections 2.2 and 4.1

2 Spiral spin liquids: Classification and model construction

The basic structure underlying spiral spin liquids is the continuous spiral manifold formed by the propagation wavevectors of the classical ground states in reciprocal space. The continuity of this spiral manifold reflects the massive ground-state degeneracy and promises a spiral spin liquid. As will be shown later, the relationship between the dimensions and codimensions of the spiral manifold is crucial for the physical properties of the systems. The codimension d_c of the spiral manifold is defined as the difference between the dimension of the system and the dimension (d_s) of the spiral manifolds, and the spiral spin liquids are classified based on (d_s, d_c) . For example, the well-known J_1 - J_2 model on the diamond lattice for MnSc_2S_4 has a degenerate spiral surface with a dimension of $d_s = 2$, and the codimension of this spiral surface is $d_c = 1$. This physical classification is listed in Table 1. In this section, specific models are proposed to explicitly demonstrate the existence of other classes and study their physical properties. The square, honeycomb, and AB-stacked multilayered triangular lattices are analyzed in detail.

2.1 Class with $d_s = 1$ and $d_c = 1$

First, a generic J_1 - J_2 Heisenberg model on the bipartite lattices with the following form is considered:

$$H = \frac{1}{2} \sum_{i,j} [J_1 \mathbf{M}_{ij} + J_2 (\mathbf{M}^2 - z\mathbb{I})_{ij}] \mathbf{S}_i \cdot \mathbf{S}_j, \quad (1)$$

where \mathbf{S}_i is the classical three-component spin vector with unit length. \mathbf{M} is a symmetric adjacency matrix of the underlying lattice, defined as

$$\mathbf{M}_{ij} = \mathbf{M}_{ji} = \begin{cases} 1 & \text{for } \langle ij \rangle, \\ 0 & \text{otherwise,} \end{cases} \quad (2)$$

where $\langle ij \rangle$ refers to the bond connecting the nearest-neighbor sites i and j , \mathbb{I} represents the identity matrix, and z is the coordination number of the lattice. The geometric meaning of $\mathbf{M}^2 - z\mathbb{I}$ is clear. Since $(\mathbf{M}^2)_{ij} = \sum_k \mathbf{M}_{ik} \mathbf{M}_{kj}$, $(\mathbf{M}^2)_{ij}$ essentially counts the number of different paths hopping from site i to site j via two nearest-neighbor bonds. When $(\mathbf{M}^2)_{ii} = z\mathbb{I}$, this represents the processes hopping back to the starting site. Therefore, these returning processes are subtracted from \mathbf{M}^2 . Hereafter, it is assumed that the antiferromagnetic interactions are $J_1 > 0$ and $J_2 > 0$. The regime with $J_1 < 0$ and $J_2 > 0$ can be achieved by only flipping spins in one sublattice, and there is no frustration when $J_2 < 0$. It will be seen that this model encodes the essential ingredients of the spiral manifold, and can be constructed on different lattices.

The well-known Luttinger–Tisza method is employed to explore the ground states of the classical J_1 - J_2 Heisenberg model in Eq. (1). The core of this method is softening the local unit-length constraint on classical spin vectors $\mathbf{S}_i^2 = 1$ by a global constraint $\sum_i |\mathbf{S}_i|^2 = N$, where N is the total number of spins. After this replacement, the original problem is reduced to minimizing the energy

$$E_{\text{LT}} = H - \lambda \left(\sum_i |\mathbf{S}_i|^2 - N \right), \quad (3)$$

where λ is a Lagrange multiplier. Fourier transformation is implemented on each spin vector with the sublattice index μ and unit-cell index i as

$$\mathbf{S}_i^\mu = \frac{1}{\sqrt{N/2}} \sum_{\mathbf{k}} \mathbf{S}_{\mathbf{k}}^\mu e^{i\mathbf{k} \cdot \mathbf{r}_i}. \quad (4)$$

Then, the energy in reciprocal space reads

$$E_{\text{LT}} = \sum_{\mathbf{k}} \left[\frac{1}{2} \mathcal{J}_{\mu\nu}(\mathbf{k}) - \lambda \delta_{\mu\nu} \right] \mathbf{S}_{\mathbf{k}}^\mu \mathbf{S}_{-\mathbf{k}}^\nu + \lambda N, \quad (5)$$

where $\mathcal{J}_{\mu\nu}(\mathbf{k})$ is the Fourier transformation of the interaction matrix defined by the adjacency matrix \mathbf{M} in real space. For the model proposed here, it has the simple form

$$\mathcal{J}(\mathbf{k}) = \begin{pmatrix} J_2 (\Lambda(\mathbf{k})^2 - z) & J_1 \Lambda(\mathbf{k}) e^{i\theta(\mathbf{k})} \\ J_1 \Lambda(\mathbf{k}) e^{-i\theta(\mathbf{k})} & J_2 (\Lambda(\mathbf{k})^2 - z) \end{pmatrix},$$

where the parameter $\Lambda(\mathbf{k}) = \left| \sum_{\mathbf{R}_{\text{NN}}} e^{-i\mathbf{k} \cdot \mathbf{R}_{\text{NN}}} \right|$. \mathbf{R}_{NN} denotes the nearest-neighbor vectors and $\theta(\mathbf{k})$ refers to the phase shift between two sublattices. Now, minimizing the energy E_{LT} is equivalent to finding the minimum eigenvalue of a quadratic form $\mathcal{J}(\mathbf{k})$. It is found that the eigenvalues form two bands with dispersions as

$$\omega_{\pm} = J_2 \left[\Lambda(\mathbf{k}) \pm \frac{J_1}{2J_2} \right]^2 - \frac{J_1^2 + 4zJ_2^2}{4J_2}. \quad (6)$$

A phase transition occurs at $J_2/J_1 = 1/(2z)$. When $J_2/J_1 < 1/(2z)$, ω_- takes its minimum at the Γ point in reciprocal space, corresponding to the antiferromagnetic Néel ordered state for the bipartite lattices. With increasing J_2/J_1 , a massive ground-state degeneracy emerges and manifests itself as a spiral manifold determined by

$$\Lambda(\mathbf{k}) = \frac{J_1}{2J_2}. \quad (7)$$

The spin configuration is then decoded from the corresponding eigenvectors. Given a wavevector \mathbf{Q} that resides on the degenerate manifold, the ground-state spin configuration in real space takes a spiral form,

$$\mathbf{S}_i^\mu = (-1)^\mu \cos[\mathbf{Q} \cdot \mathbf{r}_i + (-1)^\mu \theta(\mathbf{Q}/2)] \mathbf{e}_1 + (-1)^\mu \sin[\mathbf{Q} \cdot \mathbf{r}_i + (-1)^\mu \theta(\mathbf{Q}/2)] \mathbf{e}_2, \quad (8)$$

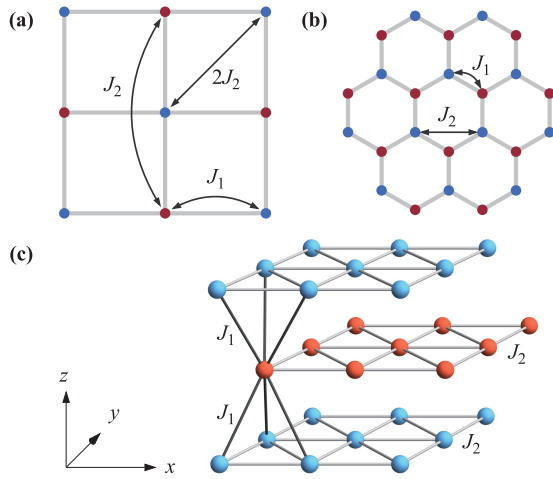


Fig. 2 (a) Square, (b) honeycomb, and (c) AB-stacked multilayered triangular lattices with J_1 and J_2 spin-exchange interactions. Sublattices are colored red and blue. Only inter-layer bonds for one site are plotted in (c) for clarity. Lattice geometries and crystal momenta are defined in Appendix A.

where μ can take 0 and 1 for two sublattices, respectively. $\mathbf{e}_{1,2}$ are any two orthogonal unit vectors.

In this subsection, the class with $d_s = 1$ and $d_c = 1$ is studied, where the spiral manifold is a contour in reciprocal space. In this class, the dimension of the system is 2. To achieve this, only one constraint on the spiral wavevector is needed to force the spins onto the spiral manifold for the classical ground states. The square and honeycomb lattices are explicitly presented as examples that are shown in Figs. 2(a) and (b). The square and honeycomb lattices are both bipartite and have the coordination numbers $z = 4$ and $z = 3$, respectively. The nearest-neighbor interaction J_1 and the next-nearest-neighbor interaction J_2 are considered for both lattices. In addition, a third nearest-neighbor interaction with the same strength of J_2 for the square lattice is involved to satisfy the definition of the adjacency matrix on the square lattice. The resulting spiral contour parameters are

$$\Lambda(\mathbf{k}) = 4 \left| \cos(\mathbf{a}_1 \cdot \frac{\mathbf{k}}{2}) \cos(\mathbf{a}_2 \cdot \frac{\mathbf{k}}{2}) \right| \quad (9)$$

for the square lattice and

$$\Lambda(\mathbf{k}) = \left[3 + 2 \cos(\mathbf{a}_1 \cdot \mathbf{k}) + 2 \cos(\mathbf{a}_2 \cdot \mathbf{k}) + 2 \cos[(\mathbf{a}_1 - \mathbf{a}_2) \cdot \mathbf{k}] \right]^{\frac{1}{2}} \quad (10)$$

for the honeycomb lattice. Here, \mathbf{a}_1 and \mathbf{a}_2 are the lattice vectors defined in Appendix. A. In Figs. 3(a) and 4(a), the spiral contours for the two lattices and their evolution with increasing J_2/J_1 are plotted. It is shown that both two spiral contours emerge at $J_2/J_1 = 1/(2z)$ from the Γ point and expand towards the boundary of the respective Brillouin zones. Despite this similarity, the spiral contours of two lattices behave dramatically differently in

the large- J_2/J_1 regime. For the square lattice, the spiral contour approaches the boundary continuously, but does not touch it until the $J_2/J_1 \rightarrow \infty$ limit, where the spiral contour completely coincides with the Brillouin-zone boundary. Physically, in this limit the proposed generic J_1 - J_2 Heisenberg model on the square lattice reduces to a conventional one with the largest frustration, and the massive degeneracy of the ground states remains. On the contrary, the spiral contour of the honeycomb lattice [18] touches the M point and other symmetry-related points in reciprocal space at $J_2/J_1 = 1/2$, and then splits into six arcs. These arcs are symmetry equivalent and can be viewed as closed loops centered at the K points. They shrink with increasing J_2/J_1 and finally become isolated points residing at point K . This means that the ground-state degeneracy disappears and Néel ordering is restored. Actually, in the $J_2/J_1 \rightarrow \infty$ limit, the two sublattices of the honeycomb lattice can be decoupled into two antiferromagnets on the triangular lattice, which is consistent with the present results. Therefore, the most important difference of these two types of lattices is whether the largest frustration state can be achieved at finite J_2/J_1 , where the spiral contour has the largest circumference.

2.2 Class with $d_s = 1$ and $d_c = 2$

The class with $d_s = 1$ and $d_c = 2$ leads to a spiral contour on a three-dimensional lattice. Such a model can be constructed from a two-dimensional bipartite lattice. Specif-

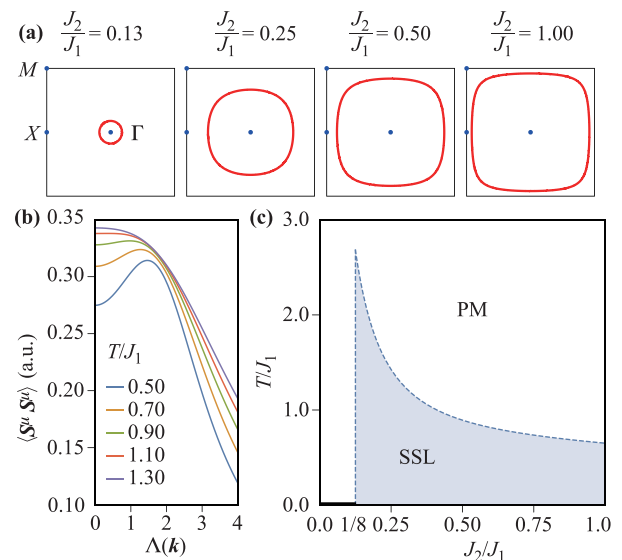


Fig. 3 Square lattice. (a) Evolution of spiral contour (red) with couplings in the first Brillouin zone. High-symmetry \mathbf{k} points are marked as blue dots. (b) Spin correlation as a function of $\Lambda(\mathbf{k})$ at different temperatures. Here, $J_2/J_1 = 0.3$ is fixed and the spin correlation is peaked at $\Lambda(\mathbf{k}) = 5/3$. (c) Phase diagram with temperature. Spiral spin liquid (SSL) regime is outlined in the paramagnetic phase (PM). Black line refers to Néel ordered state.

ically, the honeycomb lattice is decoupled into two triangular sub-systems according to its sublattices. The sublattice layers are then stacked alternatively into a three-dimensional multilayered system, as shown in Fig. 2(c). This is known as AB stacking. Here, the projection of a site from one layer onto its adjacent layer is located at the center of the triangles. The spin Hamiltonian retains the J_1 - J_2 Heisenberg form

$$H = J_1 \sum_{i,j} \mathbf{S}_i \cdot \mathbf{S}_j + J_2 \sum_{i,j} \mathbf{S}_i \cdot \mathbf{S}_j, \quad (11)$$

where $J_1 > 0$ ($J_2 > 0$) then becomes the interlayer (intralayer) interaction. Repeating the process of the Luttinger-Tisza method, it is found that the interaction matrix is

$$\mathcal{J}(\mathbf{k}) = \begin{bmatrix} J_2 \left(\frac{1}{4} \Lambda(\mathbf{k}_{\parallel})^2 - 3 \right) & J'_1 \Lambda(\mathbf{k}_{\parallel}) e^{i\theta(\mathbf{k})} \\ J'_1 \Lambda(\mathbf{k}_{\parallel}) e^{-i\theta(\mathbf{k})} & J_2 \left(\frac{1}{4} \Lambda(\mathbf{k}_{\parallel})^2 - 3 \right) \end{bmatrix}, \quad (12)$$

where $\mathbf{k}_{\parallel} = \{k_x, k_y, 0\}$ and $J'_1 = J_1 \cos(\frac{1}{2} \mathbf{a}_3 \cdot \mathbf{k})$ with the lattice vectors \mathbf{a}_i defined in Appendix A. The explicit form of $\Lambda(\mathbf{k}_{\parallel})$ is expressed as

$$\Lambda(\mathbf{k}) = 2 \left[3 + 2 \left[\cos(\mathbf{a}_1 \cdot \mathbf{k}_{\parallel}) + \cos(\mathbf{a}_2 \cdot \mathbf{k}_{\parallel}) \right] + \cos \left[(\mathbf{a}_1 - \mathbf{a}_2) \cdot \mathbf{k}_{\parallel} \right] \right]^{\frac{1}{2}}. \quad (13)$$

The minimum eigenvalue of $\mathcal{J}(\mathbf{k})$,

$$\omega_- = \frac{J_2}{4} \left[\Lambda(\mathbf{k}_{\parallel}) - \frac{2J'_1}{J_2} \right]^2 - \frac{J_1'^2 + 3J_2^2}{J_2}, \quad (14)$$

defines a spiral contour

$$\Lambda(\mathbf{k}_{\parallel}) = \frac{2J_1}{J_2}, \quad (15)$$

on the $k_z = 0$ plane when $J_2/J_1 > 1/3$. Before the spiral contour emerges, an antiferromagnetic Néel ordering is favored. As depicted in Fig. 5, the evolution of the spiral contour is very similar to that of the honeycomb lattice shown in Fig. 4(a). Nevertheless, the critical value at which the spiral contour touches the M points and is reconstructed becomes $J_2/J_1 = 1$. This can be attributed to the layer structure with doubling interlayer (inter-sublattice) bonds compared to the honeycomb lattice.

2.3 Examples with $d_c = 0$

In addition to the classes listed in Table 1, there exist examples with $d_c = 0$. The well-known cases are the classical Kagomé lattice Heisenberg model and classical pyrochlore lattice Heisenberg model. Because of the local zero-energy modes, the classical ground state has extensive degeneracy. The lowest eigenvalue of the exchange matrix in reciprocal space has no dispersion. The flatness arises from the existence of local zero-energy modes

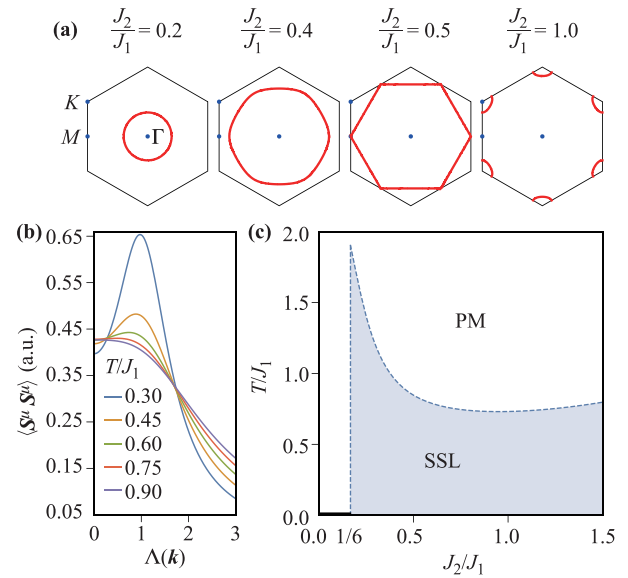


Fig. 4 Honeycomb lattice. (a) Evolution of spiral contour (red) with couplings in the first Brillouin zone. High-symmetry \mathbf{k} points are marked as blue dots. (b) Spin correlation as a function of $\Lambda(\mathbf{k})$ at different temperatures. Here, $J_2/J_1 = 0.5$ is fixed where the spin correlation is peaked at $\Lambda(\mathbf{k}) = 1$. (c) Phase diagram with temperature. Spiral spin liquid (SSL) regime is outlined in the paramagnetic phase (PM). Black line refers to Néel ordered state.

on each hexagon plaquette in the ground-state manifold. It is better to understand the classical ground state in the real-space picture. The classical ground state requires that each triangular plaquette of the Kagomé lattice has a total spin equal to zero. This is like a Gauss's law constraint for electromagnetism. In fact, the low-temperature magnetic properties can be well captured by an emergent classical electromagnetism that gives rise to a power-law spin correlation with a dipolar-like angular dependence. The classical pyrochlore lattice Heisenberg model was understood in a similar fashion. For the above reason, these two $d_c = 0$ examples are not included in the current study of spiral spin liquids.

3 Finite-temperature behaviors

In the preceding section, the similarity and difference between different classes of spiral spin liquids were discussed. Next, the finite-temperature behaviors of the spiral spin liquid regime are explored. A crucial difference here is the existence of ordered states due to the thermal order-by-disorder in the three spatial dimensions, which is prohibited in two spatial dimensions by the well-known Mermin-Wagner theorem. These ordered states can only persist in the rather low-temperature regime in three dimensions. In general, the increasing thermal fluctuation will eventually favor a disordered state as temperature increases. It

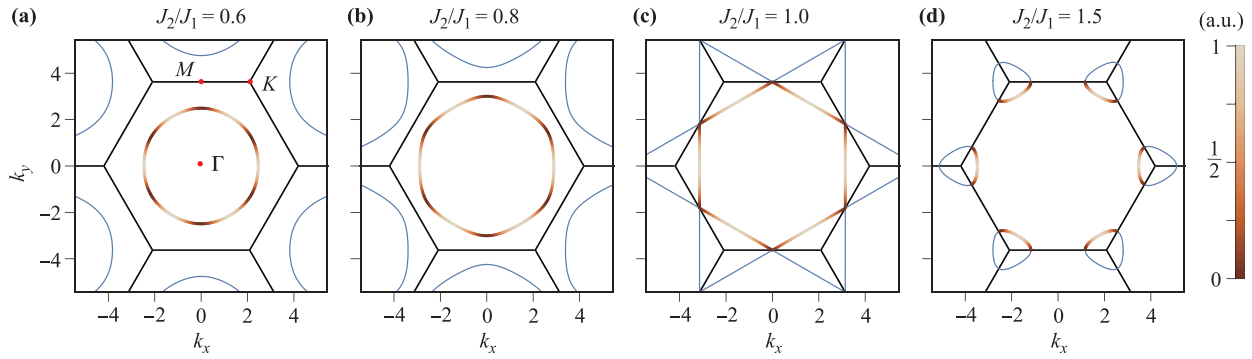


Fig. 5 Spiral contour for AB-stacked multilayered triangular lattice with different J_2/J_1 on the $k_z = 0$ plane. Black lines refer to the Brillouin-zone boundaries. High-symmetry \mathbf{k} points are marked as red dots. In the first Brillouin zone, the spiral contours are colored according to the relative magnitudes of the free energy.

will be shown that a broad range of the spiral spin liquid regime can persist before crossing over to the trivial paramagnetic regime.

3.1 Spiral spin liquid regime

The presence of the massive ground-state degeneracy, i.e., the spiral surface manifold, will affect the finite-temperature behavior of the system by revealing itself in different ways in different temperature regimes. For two spatial dimensions, the Mermin–Wagner theorem implies the absence of long-range order at finite temperatures, and there should be a wide regime in which the spiral spin liquid dominates the physics down to zero temperature when $J_2/J_1 > (J_2/J_1)_c$. The stability of the spiral spin liquid regime can be extended to the three-dimensional case, except that ordered states may exist at a sufficiently low temperature, which will be explained later. Here, the spiral spin liquid regime is characterized by the strong peaks of the spin-spin correlation in reciprocal space, located exactly on the spiral manifold. As the thermal fluctuation increases, these peaks will gradually become flat and broad, and will eventually become invisible in the trivial paramagnetic limit. To elucidate the regime of the spiral spin liquid, the spin correlation function at high temperatures is calculated by the self-consistent Gaussian approximation. Under the global constraint as introduced in Section 2, the partition function of the spin system is given by

$$\mathbb{Z} = \int \mathcal{D}\mathbf{S}\mathcal{D}\lambda e^{-\beta H - i\lambda(\sum_i S_i^2 - N)}, \quad (16)$$

where λ is the Lagrange multiplier to enforce $\sum_i S_i^2 = N$. This is also known as the spherical approximation [7]. The saddle-point solution can be obtained by integrating out the classical spins, and the effective action scales as N that naturally leads to the saddle-point solution for λ . The saddle-point solution is taken by replacing $i\lambda \rightarrow \beta\lambda'(T)/2$, where $\lambda'(T)$ is a saddle-point parameter to be determined self-consistently. Equivalently, the saddle-point equation

can be obtained from the spherical constraint for the spins,

$$\begin{aligned} \sum_i \mathbf{S}_i^2 &= \sum_{\mu} \sum_{\mathbf{k}} S_{\mathbf{k}}^{\mu} S_{-\mathbf{k}}^{\mu} \\ &= \sum_{\mathbf{k}} \frac{3}{\beta} \left[\frac{1}{\omega_{-}(\mathbf{k}) + \lambda'(T)} + \frac{1}{\omega_{+}(\mathbf{k}) + \lambda'(T)} \right] \\ &\equiv N, \end{aligned} \quad (17)$$

where the spin-correlation function in reciprocal space for the spins from the same sublattice μ is

$$\langle S_{\mathbf{k}}^{\mu} S_{-\mathbf{k}}^{\mu} \rangle = \frac{1}{2\beta} \left[\frac{1}{\omega_{-}(\mathbf{k}) + \lambda'(T)} + \frac{1}{\omega_{+}(\mathbf{k}) + \lambda'(T)} \right], \quad (18)$$

and ω_{\pm} refers to the two branches of eigenvalue dispersions of the exchange-interaction matrix $\mathcal{J}(\mathbf{k})$ defined in Section 2. One can obtain the parameter $\lambda'(T)$ by solving the above saddle-point equation. In Figs. 3(b) and 4(b), the temperature dependence of the spin correlation $\langle S_{\mathbf{k}}^{\mu} S_{-\mathbf{k}}^{\mu} \rangle$ is depicted as a function of $\Lambda(\mathbf{k})$ for the square and honeycomb lattices. The peaks correspond to points near the spiral contour that are apparent and remain discernible up to a crossover temperature. The spiral spin liquid regime can then be roughly identified by tracing this feature. The crossover between the spiral spin liquid regime and conventional high-temperature paramagnet regime is outlined in Figs. 3(c) and 4(c). It is shown that the frustration from the competing spin interactions can manifest itself qualitatively through this crossover temperature. The enhancement of frustration will strongly suppress the spiral spin liquid physics and make it easier for the system to enter a trivial paramagnetic state under the thermal fluctuation. In proximity to ordered states, a spiral spin liquid can persist up to a higher temperature. Since the largest frustration for the square lattice appears in the $J_2/J_1 \rightarrow \infty$ limit, a monotonically decreasing crossover temperature is obtained, in contrast to the honeycomb-lattice case in which there is a minimal crossover temperature near $J_2/J_1 = 1/2$. The spiral spin liquid regime is

a special paramagnetic phase in which the spiral manifold governs the thermal fluctuations.

The finite-temperature behaviors for three dimensions have no qualitative difference. For the proposed AB-stacked multilayered triangular lattice, the spiral spin liquid regime and its crossover to the trivial paramagnet resemble those of the honeycomb lattice. The difference is that, in the low-temperature regime, the spiral ordered states can emerge through the thermal order-by-disorder mechanism. This is discussed in the next subsection.

3.2 Thermal order-by-disorder

Although the ground-state configuration can fluctuate on the degenerate spiral manifold without any energy cost at zero temperature, a global selection among these ground states will occur when weak thermal fluctuation is considered. At finite temperatures, the free energies of the degenerate ground states are usually different. To minimize the free energy, certain spiral ordered states associated with large entropy are selected. This stabilization mechanism of long-range order driven by the entropy is termed thermal order-by-disorder. This effect for the AB-stacked multilayered triangular lattice model is studied in the low-temperature regime.

First, a spiral spin order at momentum \mathbf{q} with a spin configuration $\bar{\mathbf{S}}$ lying in the x - y plane is assumed and then its local stability is analyzed. The fluctuations can be parameterized as

$$\boldsymbol{\phi} = \phi^o \hat{\mathbf{z}} + \phi^i [\hat{\mathbf{z}} \times \bar{\mathbf{S}}], \quad (19)$$

where ϕ^o and ϕ^i are out-of-plane and in-plane fluctuations, respectively. Physical spins can be expressed in fluctuation variables around the assumed order as

$$\mathbf{S} = \boldsymbol{\phi} + \bar{\mathbf{S}}(1 - \phi^2)^{1/2}. \quad (20)$$

The unit-vector constraint remains satisfied since $\boldsymbol{\phi} \cdot \bar{\mathbf{S}} = 0$. For $\phi^2 \ll 1$, one can safely expand the spin Hamiltonian (11) in a fluctuation field up to second order,

$$H = \frac{1}{2} \sum_{ij} \tilde{J}_{ij} \phi_i^o \phi_j^o + \tilde{J}_{ij} (\bar{\mathbf{S}}_i \cdot \bar{\mathbf{S}}_j) \phi_i^i \phi_j^i. \quad (21)$$

Here, $\tilde{J}_{ij} = J_{ij} - \delta_{ij} \omega_-^{\min}$. The shift makes both eigenvalues non-negative and only scales the partition function by a constant. There is no change in free energy, except for a zero-point movement. The zeroth- and first-order Hamiltonians have also been ignored because the former is just the ground-state energy and the latter should vanish in an ordered state. The resulting partition function is

$$\mathcal{Z} = \int \mathcal{D}\boldsymbol{\phi} e^{-\beta H} (1 - \phi^2)^{-1/2} \propto \int \mathcal{D}\phi^o \mathcal{D}\phi^i e^{-\mathcal{S}}, \quad (22)$$

where the action is $\mathcal{S} = \beta H$. In the last step, a Jacobian factor is dropped since $(1 - \phi^2)^{-1/2} \approx e^{(\phi^o{}^2 + \phi^i{}^2)/2}$

up to second order. That means that this factor only contributes diagonal terms to the action and does not affect the relative magnitude of free energy. At the Gaussian level, two components of the fluctuation field are decoupled. The out-of-plane fluctuation modes ϕ^o have zero modes for all momenta on the spiral manifold and thus are responsible for the massive ground-state degeneracy. The in-plane fluctuation modes ϕ^i , however, have only one single gapless mode and are well-behaved at low temperature. The gapless mode is just the Goldstone mode required by symmetries and indicates a long-range order.

For the proposed J_1 - J_2 Heisenberg model on the AB-stacked multilayered triangular lattice, these ϕ^i fluctuation modes with spiral ordering wavevector \mathbf{q} are

$$\begin{aligned} \gamma_{\pm}(\mathbf{k}, \mathbf{q}) = & \frac{J_2}{8} (|\xi_+|^2 + |\xi_-|^2 - 24) - \omega_-^{\min} \\ & \pm \frac{J_1}{2} \left| \xi_+ \cos \frac{\mathbf{a}_3 \cdot (\mathbf{k} + \mathbf{q})}{2} + \xi_- \cos \frac{\mathbf{a}_3 \cdot (\mathbf{k} - \mathbf{q})}{2} \right|, \end{aligned} \quad (23)$$

where $\xi_{\pm} = \Lambda(\mathbf{k}_{\parallel} \pm \mathbf{q}) e^{\mp i\theta(\mathbf{q}) + i\theta(\mathbf{k} \pm \mathbf{q})}$. Therefore, one can integrate the fluctuation fields to obtain the \mathbf{q} -dependent part of free energy,

$$F_{\phi^i}(\mathbf{q}) = T \int_{\mathbf{k}} [\ln \gamma_+(\mathbf{k}, \mathbf{q}) + \ln \gamma_-(\mathbf{k}, \mathbf{q})] / (2\pi T). \quad (24)$$

The free-energy distribution on the spiral contour is visualized as shown in Fig. 5, in which the color reflects the relative magnitude of $F_{\phi^i}(\mathbf{q})$. Once the spiral contour emerges, the free-energy minima arise at $(0, q, 0)$ and symmetry-related points, indicating a phase transition from Néel order to spiral order. When the spiral contour touches the Brillouin-zone boundary at $J_2 = J_1$, the minima locate at M points and move towards K points as J_2/J_1 increases. In the $J_2/J_1 \rightarrow \infty$ limit, two decoupled antiferromagnetic magnets on triangular lattices are obtained, as expected.

The spiral ordering selected by entropy will melt when the system leaves the low-temperature regime. Above a critical temperature T_c , the spiral spin liquid behavior prevails again. To construct a finite-temperature phase diagram for spin orderings, classical Monte Carlo simulations are carried out on the AB-stacked multilayered triangular lattice with L^3 unit cells. Owing to strong frustrations, a simple Metropolis-Hastings update will have a very long auto-correlation time that would lead to non-ergodicity. Here, a generally applicable method, parallel tempering [27], is employed to resolve this issue. Essentially, in parallel tempering the simulated space consists of several replicas of the systems while they are at different temperatures. Exchanging configurations in different replicas will decrease or increase the total energy according to the detailed balance, and there is an acceptance probability for this update. Therefore, the configurations of the high-temperature replicas can be tunneling to the lower-temperature replicas and vice versa. This diffusion

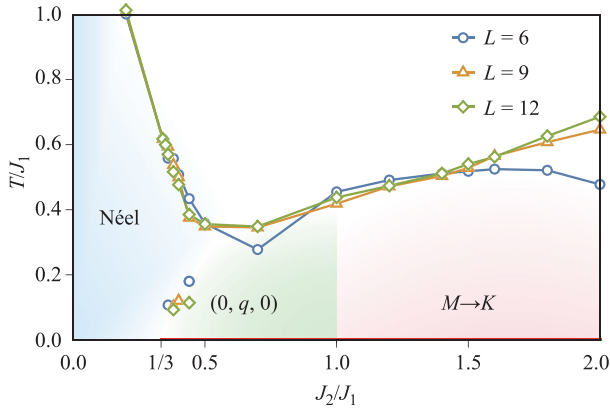


Fig. 6 Phase diagram for AB-stacked multilayered triangular lattice in low-temperature regime. In addition to Néel order, two types of spiral order are identified in agreement with the current thermal order-by-disorder analysis. The ordering temperatures T_c are determined to be locations of specific-heat peaks by classical Monte Carlo simulations for systems with $L = 6, 9, 12$. Near the critical value of $J_2/J_1 = 1/3$, a re-entrant of Néel order occurs. Red line refers to spiral spin liquid phase at zero temperature.

process will significantly improve the efficiency. Furthermore, the over-relaxation method is employed to further decrease the auto-correlation time as well. The finite-temperature phase boundary can be determined by the grown peak of the specific heat with increasing system size, and the numerical results are shown in Fig. 6. Compared to the rapidly declining boundary of Néel order, T_c has a slower growth in the spiral order phases. The lowest critical temperature also occurs near the largest frustration area. Moreover, it is found that thermal fluctuation stabilizes the Néel phase even slightly above $J_2/J_1 = 1/3$, and thus induces re-entrant behavior. This subtle boundary exposes the intricate competitions between the spin interactions and thermal fluctuation in spiral spin liquid systems.

3.3 Specific heat

As mentioned previously, different classes of spiral spin liquids could exhibit distinct behaviors at low temperatures. In addition to the spin correlations, these distinctions can be directly reflected in the thermodynamic quantities. To demonstrate, here the specific heats C_v for the spiral spin liquids with $(d_s, d_c) = (1, 1)$ and $(1, 2)$ respectively, are calculated.

In two-dimensional systems, the spiral spin liquid can persist down to zero temperature. In the low-temperature regime, fluctuations near the spiral contour govern the physics and the minimum eigenvalue mode vanishes for momenta on the spiral contour. Therefore, the self-consistent equation (17) can be approximated as

$$\int_{\mathbf{k}} \frac{1}{\omega_{-}(\mathbf{k}) + T^{\alpha} \bar{\lambda}} \sim \frac{2}{3} \beta. \quad (25)$$

Here, it is assumed that the saddle-point solution has a power-law temperature dependence as $\lambda'(T) \sim T^{\alpha} \bar{\lambda}$. At low temperatures, the integral can be well estimated by considering momenta near the spiral contour. For a momentum \mathbf{q} located on the spiral contour, a coordination framework spanned by the normal vector $\hat{\mathbf{n}}$ and the tangent vector $\hat{\mathbf{t}}$ can be associated. Along the normal direction, the dispersion of the minimum eigenvalue mode can be replaced by $\omega_{-}(\mathbf{k}) = v(\delta p)^2$, where $\delta p = (\mathbf{k} - \mathbf{q}) \cdot \hat{\mathbf{n}}$ and $\mathbf{k} \cdot \hat{\mathbf{t}} = 0$. The integral can be taken over δp with a proper cutoff and over the contour itself. By modifying the variable $\delta p = T^{\alpha/2} x$, one can scale out the power $\alpha = 2$ for the saddle-point solution $\lambda'(T)$.

The free energy $F = -T \ln \mathcal{Z}$ in this approximation is

$$F \approx -\frac{1}{2} T^2 \bar{\lambda} + \frac{1}{2} T \int_{\mathbf{k}} \ln[(\omega_{-}(\mathbf{k}) + T^2 \bar{\lambda}) / (2\pi T)]. \quad (26)$$

To calculate the specific heat $C_v = -T (\partial^2 F / \partial T^2)_{V, N}$, it is convenient to consider

$$\frac{\partial(F/T)}{\partial T} = -\frac{\bar{\lambda}}{2} - \frac{1}{4\pi T} + \int_{\mathbf{k}} \frac{T \bar{\lambda}}{\omega_{-}(\mathbf{k}) + T^2 \bar{\lambda}} \approx \frac{c_1}{T} + c_2. \quad (27)$$

In the last step, the self-consistent equation is used to finish the integral. Thus, the free energy has the form $F = c_1 T \ln T + c_2 T^2 + c_3 T$, and the specific heat is expressed as

$$C_v = c_1 + c_2 T. \quad (28)$$

Here, c_1 and c_2 are new constants absorbing all coefficients.

For spiral spin liquids in three spatial dimension, the development of spiral orderings in the low-temperature regime has significant effects on the thermodynamic quantities. In the absence of the thermal order-by-disorder, the dispersions of fluctuation modes from out-of-plane field ϕ^o are $\omega_{\pm}(\mathbf{k}) - \omega_{-}^{\min}$ at the Gaussian level and the lowest one vanishes for any momentum on the spiral contour. This inevitably leads to a divergence of the fluctuation amplitude proportional to $T \int_{\mathbf{k}} 1/G_0(\mathbf{k})$, where $G_0(\mathbf{k})$ is the propagator of ϕ^o . To cure the divergence, one must consider higher-order terms in the expression of fluctuation fields ϕ^i and ϕ^o . Their contributions can be formally treated as a self-energy correction $\Sigma(\mathbf{k})$, giving rise to the Green's function

$$G(\mathbf{k}) = \frac{1}{\omega_{\pm}(\mathbf{k}) - \omega_{-}^{\min} + \Sigma(\mathbf{k})}. \quad (29)$$

With the aid of the diagrammatic perturbation theory, $\Sigma(\mathbf{k})$ can be expressed self-consistently as

$$\Sigma(\mathbf{k}) = T \int_{\mathbf{p}} D(\mathbf{k}, \mathbf{p}) G(\mathbf{p}), \quad (30)$$

where $D(\mathbf{k}, \mathbf{p})$ is a well-behaved function and vanishes only at finite momenta corresponding to the Goldstone

modes. Therefore, the dominant contribution of the integral still comes from momenta near the spiral contour. The numerator of the integrand is thus replaced by $D(\mathbf{k}, \mathbf{q})$, where \mathbf{q} denotes the momentum on the contour. Similarly, one can associate the point \mathbf{q} with a coordination framework spanned by the normal vector $\hat{\mathbf{n}}$, the tangent vector $\hat{\mathbf{t}}$, and the original z -axis vector $\hat{\mathbf{z}}$. In the $\hat{\mathbf{n}}-\hat{\mathbf{z}}$ plane, the dispersion of the eigenvalue mode $\omega_-(\mathbf{p}) - \omega_{\min}$ is still quadratic. One can parameterize momentum \mathbf{p} in this plane as $\mathbf{p} \cdot \hat{\mathbf{n}} = \delta p \cos \theta$ and $\mathbf{p} \cdot \hat{\mathbf{z}} = \delta p \sin \theta$, where $\mathbf{p} \cdot \hat{\mathbf{t}} = 0$ and $\delta p = |\mathbf{p} - \mathbf{q}|$. The dispersion of the minimum eigenvalue mode can then be expressed as $v^2(\delta p)^2$ approximately. It is further assumed that the self-energy has a temperature dependence with the leading form $\Sigma(\mathbf{k}) = T^\alpha \Sigma'(\mathbf{k})$ due to the thermal splitting. The self-consistent equation reduces to

$$T^\alpha \Sigma'(\mathbf{k}) = T \int_{\mathbf{p}} \frac{D(\mathbf{k}, \mathbf{q})}{v^2(\delta p)^2 + T^\alpha \Sigma'(\mathbf{q})}. \quad (31)$$

The integral is taken on the $\hat{\mathbf{n}}-\hat{\mathbf{z}}$ plane with respect to θ and δp with a proper cutoff, and over the contour itself. Modifying the variables as $\delta r = \delta p/T^{\alpha/2}$, the stiffness T^α can be scaled out of the integral and one obtains $\alpha = 1$.

The full free energy should include both the ϕ^i and ϕ^o parts, and be corrected by the self-energy as well. Up to the order of T , it takes the form

$$\begin{aligned} F &= F_{\phi^i}(\mathbf{q}) + T \int_{\mathbf{k}} \ln[(\omega_{\pm}(\mathbf{k}) - \omega_{\min} + T\Sigma'(\mathbf{k})) / (2\pi T)] \\ &= c_1 T \ln T + T \int_{\mathbf{k}} \ln[\omega_{\pm}(\mathbf{k}) - \omega_{\min} + T\Sigma'(\mathbf{k})] + c_3 T. \end{aligned} \quad (32)$$

To calculate the specific heat, the following equation is evaluated:

$$\frac{\partial(F/T)}{\partial T} = \frac{c_1}{T} + \int_{\mathbf{k}} \frac{\Sigma'(\mathbf{k})}{\omega_{\pm}(\mathbf{k}) - \omega_{\min} + T\Sigma'(\mathbf{k})}. \quad (33)$$

Repeating the same scaling trick, it is found that the temperature dependence of free energy $F = c_1 T \ln T + c_2 T^2 + c_3 T$, and thus the low-temperature specific heat is

$$C_v = c_1 + c_2 T. \quad (34)$$

We have absorbed all coefficients into c_1 and c_2 and they should not be confused with the previous constants.

4 Discussion

4.1 Survey of materials

A survey of existing materials is presented in which spiral spin liquid physics can be relevant. The A-site spinels AB_2X_4 represent a large family of compounds for the diamond-lattice antiferromagnets. The magnetism comes

from the A-site ions that form a diamond lattice. Among them, $MnSc_2S_4$ and $CoAl_2O_4$ manifest the strongest frustration of classical spins and are suggested to support spiral spin liquids by early experimental and theoretical works [7, 28–30]. Although later measurements ruled out the possibility of $CoAl_2O_4$ as a candidate [31], in recent experiments the spiral surface in $MnSc_2S_4$ was directly observed by neutron-scattering measurements and proved the existence of a spiral spin liquid regime for the spin-5/2 Mn^{2+} ions [11]. Instead of an ordering transition via the thermal order-by-disorder, a multi-step ordering behavior was observed at low temperatures. This reveals the limitation of the J_1-J_2 Heisenberg model and suggests that more interactions should be considered, such as the third-nearest-neighbor coupling in real materials [8, 32]. Other spinels like ARh_2O_4 ($A = Ni, Co,$ and Cu) and $MgCr_2O_4$ have also been synthesized recently [14, 33–35]. For $NiRh_2O_4$ with frustrated spin-1 Ni^{2+} ions, the negative Curie–Weiss temperature and absence of the magnetic ordering transition down to 0.1 K are noted. This material has spin $S = 1$ and the quantum effects seem to be strong. Quantum effects on the spiral manifold were seriously considered [35, 36]. As the material has a tetragonal symmetry rather than cubic symmetry and the Ni^{2+} has a partially filled t_{2g} shell, the single-ion anisotropy as well as the on-site spin–orbit coupling were thus also considered in addition to the superexchange interactions [35–38]. More experiments are needed to resolve the physics in $NiRh_2O_4$. The Co^{2+} ion in $CoRh_2O_4$ has $S = 3/2$, and a large nearest-neighbor exchange was found in $CoRh_2O_4$, so an Néel order was observed [34]. The Cu^{2+} ion in $CuRh_2O_4$ and $CuAl_2O_4$ has a d^9 configuration with five electrons on the upper t_{2g} shell. The spin-orbit coupling is active. It is not purely spin physics, and one would necessarily consider the orbital degree of freedom. It was noted that this Cu^{2+} ion in the tetrahedral environment is similar to the well-known Ir^{4+} ion in the octahedral environment and gives a $J_{\text{eff}} = 1/2$ local moment [37, 39, 40]. The model for these Cu^{2+} moments in $CuRh_2O_4$ would not be a simple J_1-J_2 model, so spiral spin liquid physics may not be directly relevant. This system would be better described by an anisotropic Heisenberg-compass model on the diamond lattice. This will be analyzed in future works. Recently, a rare-earth compound $LiYbO_2$ was proposed to realize a diamond lattice [15]. Its theoretical understanding was based on the effective spin-1/2 J_1-J_2 Heisenberg model with the proximity to spiral spin liquid physics and the spiral manifold despite a large spin-orbit coupling for the Yb^{3+} ions. The possible success in $LiYbO_2$ may point to the possibility of realizing a spiral spin liquid in other Yb-based systems, such as the Yb-based honeycomb-lattice magnets.

The 6H-B- $Ba_3NiSb_2O_9$ compound with a spin $S = 1$ local moment has the same structure of the AB-stacked multilayered triangular lattice model studied herein, and this material was proposed to be a spin liquid candidate [41].

It has been suggested that the quantum effect in addition to spiral contour physics plays an important role in the spin-liquid phenomenology [42]. This may inspire the study of isostructural materials with $d_s = 1$ spiral manifolds in three dimensions. The compound MgCr_2O_4 was shown to have line degeneracies in reciprocal space, and the spiral spin liquid was proposed to be relevant [14]. This again corresponds to the $d_s = 1$ case.

The relevant materials in two dimensions can be $\text{Bi}_3\text{Mn}_4\text{O}_{12}(\text{NO}_3)$ and $\text{Ca}_{10}\text{Cr}_7\text{O}_{28}$. $\text{Bi}_3\text{Mn}_4\text{O}_{12}(\text{NO}_3)$ is a bilayer honeycomb-lattice magnet with $S = 3/2$ spins and exhibits a spin-liquid-like behavior down to 0.4 K [43]. Theoretically, this observed behavior falls into the situation of massive ring-like degeneracy and an order-by-disorder mechanism in a J_1 - J_2 Heisenberg model [43, 44]. Recently, a novel ripple state under the external magnetic field has been reported and can be explained by the infinite ring-like degeneracy [12]. $\text{Ca}_{10}\text{Cr}_7\text{O}_{28}$ is another frustration magnets in which Cr^{5+} ions form a Kagomé bilayer structure. As the interaction between the Cr^{5+} spin-1/2 moment inside the triangular unit is dominantly ferromagnetic, one can treat the triangular unit as a total spin $S = 3/2$. The physics of this bilayer system can then be modeled as a semiclassical Heisenberg Hamiltonian on a honeycomb lattice with effective spin $S = 3/2$ moments and the intralayer and interlayer couplings are antiferromagnetic and ferromagnetic, respectively [16]. A ring-like pattern in the neutron-scattering signal and ordering transition at low temperature are also suggested for these materials [16, 17]. These studies suggest a particular relevance to the spiral spin liquid. However, there is still a lack of experimental results to reach a conclusion at this stage.

4.2 Open theoretical questions

Several open theoretical questions about the physics related to the spiral spin liquids are discussed here. In our calculation, the spin is treated classically. However, in reality, the spins always have quantum effects, especially for small spins. It is well known that the quantum fluctuations could break the spiral degeneracy for the ground state via the mechanism of the quantum order by disorder, and specific spiral states could be selected. The ordered states via the quantum order by disorder can sometimes be different from the thermal order by disorder. The thermal order by disorder is an entropic effect and requires a finite temperature, while the quantum order by order results from the quantum zero-point energy and works well for zero and low temperatures. This seems to suggest that there could be two thermal transitions as one cools the system from the high-temperature paramagnetic phase. The system first enters the ordered state via the thermal order by disorder and then develops another ordered phase due to the quantum order by disorder at a lower temperature. This is possible. Nevertheless, the separation of quantum

order by disorder and thermal order by disorder is an artificial procedure, while nature blends these two effects together in the system. The blending of these effects may even favor another ordered state that differs from that favored by either. These issues may be resolved in future theoretical works.

Another important question concerns the internal spin space. All the models considered in this work have a global rotation symmetry with Heisenberg interactions and spins. The question is whether the spiral spin liquid regime can persist for XY spins or even for Ising spins. For XY spins with a $U(1)$ symmetry, it is still possible to construct spiral states with two components of the XY spins. Thus, it is natural to expect that the spiral spin liquid exists for the XY or Heisenberg spins with an easy-plane anisotropy. Moreover, the scenario for spiral spin liquids with XY spins resembles the bosonic models with frustrated hoppings, in which bosons could condense in a closed line instead of discrete points. Such phenomena have been discussed in various systems including the frustrated systems [45], high T_c superconductors [46], and driven-dissipative systems [47]. For Ising spins, it is not obvious if such a spiral spin liquid could survive as there is no way that one can construct spiral spin states with Ising spins. In contrast, the self-consistent Gaussian approximation that ignores the individual spin-magnitude constraint works rather well for the spiral spin liquid, and was known to work reasonably for certain Ising systems. Taken together, it is uncertain whether Ising spins could support the spiral spin liquid regime; this question will be addressed in a forthcoming paper.

Finally, the interplay of the quantum effect and degenerate spiral manifold may require a more systematic study in the future. Only in a few previous works, including Refs. [35–37, 48] in the diamond lattice antiferromagnet and Refs. [18, 21, 42] in the honeycomb lattice, and the AB-stacking multilayered triangular lattice, have explorations along this line been conducted. In fact, many of the spin moments in the existing materials already involve significant quantum fluctuations and could provide a good experimental platform for studying these physics.

4.3 Summary

In summary, the spiral spin liquids based on the dimension d_s and codimension d_c of the degenerate spiral manifold are classified. For each class, a minimal model based on the J_1 - J_2 Heisenberg Hamiltonian is constructed. These constructions are not unique, but essentially capture the physics of spiral spin liquids. Systematic studies are performed on the square, honeycomb, and AB-stacked multilayered triangular lattices. These lattices, together with the well-studied diamond lattice, cover all three classes in the classification presented in Table 1. The present model construction takes the bipartite lattice as a starting point. The non-Bravais lattices, like the honeycomb

and diamond lattices, have been studied and incorporated into this work and the classification. Many Bravais lattices, such as the square lattice in two dimensions, simple cubic, face-centered-cubic, and body-centered cubic lattices in three dimensions, can be treated as bipartite lattices as well once their adjacency matrices are carefully dealt with. The penalty of this straightforward extension is the requirement of further and more complicated interactions that may be rather unnatural in real materials. It is likely that some materials may be located near the unnatural parameter regime, and the additional interactions can be treated as a perturbation to break the spiral manifold. Despite this, the current classification and theoretical results depend only on the dimensions and can be immediately applied once the spiral manifold emerges.

Appendix A Lattice geometry and crystal momenta

The square lattice is regarded as a bipartite lattice with two sublattices as shown in Fig. 2(a) and one of the unit cells is chosen as a reference point with sublattice positions $(0, 0)$ and $(1, 0)$. The primitive lattice vectors are

$$\mathbf{a}_1 = (1, 1), \quad \mathbf{a}_2 = (-1, 1). \quad (\text{A1})$$

In reciprocal space, two reciprocal vectors are defined by

$$\mathbf{b}_1 = (\pi, \pi), \quad \mathbf{b}_2 = (-\pi, \pi). \quad (\text{A2})$$

The crystal momenta shown in Fig. 3(a) are

$$X = \left(\frac{\pi}{2}, \frac{\pi}{2}\right), \quad M = (\pi, 0). \quad (\text{A3})$$

For the honeycomb lattice, a unit cell containing sublattices at positions $(0, 0)$ and $(1/\sqrt{3}, 0)$ is chosen as a reference point. The primitive lattice vectors are

$$\mathbf{a}_1 = \left(\frac{\sqrt{3}}{2}, \frac{1}{2}\right), \quad \mathbf{a}_2 = \left(\frac{\sqrt{3}}{2}, -\frac{1}{2}\right), \quad (\text{A4})$$

and the reciprocal vectors are defined by

$$\mathbf{b}_1 = 2\pi \left(\frac{1}{\sqrt{3}}, 1\right), \quad \mathbf{b}_2 = 2\pi \left(\frac{1}{\sqrt{3}}, -1\right). \quad (\text{A5})$$

The crystal momenta shown in Fig. 4(b) are

$$M = 2\pi \left(\frac{1}{\sqrt{3}}, 0\right), \quad K = 2\pi \left(\frac{1}{\sqrt{3}}, \frac{1}{3}\right). \quad (\text{A6})$$

The AB-stacked multilayered triangular lattice is a hexagonal system. Two sites connected by interlayer interaction J_1 are chosen as an unit cell and their positions set to be $(0, 0, 0)$ and $(1/2, \sqrt{3}/6, c/2)$, where c is a positive constant. The primitive vectors then reads

$$\mathbf{a}_1 = (1, 0, 0), \quad \mathbf{a}_2 = \left(\frac{1}{2}, \frac{\sqrt{3}}{2}, 0\right), \quad \mathbf{a}_3 = (0, 0, 2c). \quad (\text{A7})$$

The reciprocal vectors are

$$\mathbf{b}_1 = \left(2\pi, -\frac{2\pi}{\sqrt{3}}, 0\right), \quad \mathbf{b}_2 = \left(0, \frac{4\pi}{\sqrt{3}}, 0\right), \quad \mathbf{b}_3 = \left(0, 0, \frac{\pi}{c}\right). \quad (\text{A8})$$

The crystal momenta shown in Fig. 5 are

$$M = 2\pi \left(0, \frac{1}{\sqrt{3}}, 0\right), \quad K = 2\pi \left(\frac{1}{3}, \frac{1}{\sqrt{3}}, 0\right). \quad (\text{A9})$$

Acknowledgements We thank Dr. Fei-Ye Li and Dr. Xiao-Tian Zhang for useful discussions. This work was supported by the Ministry of Science and Technology of China (Grant Nos. 2018YFE0103200, 2016YFA0300500, and 2016YFA0301001), the Shanghai Municipal Science and Technology Major Project (Grant No. 2019SHZDZX04), and the Research Grants Council of Hong Kong with General Research Fund (Grant No. 17306520).

References

1. L. Balents, Spin liquids in frustrated magnets, *Nature* 464, 199 (2010)
2. L. Savary and L. Balents, Quantum spin liquids: A review, *Rep. Prog. Phys.* 80, 016502 (2016)
3. P. A. Lee, From high temperature superconductivity to quantum spin liquid: Progress in strong correlation physics, *Rep. Prog. Phys.* 71, 012501 (2007)
4. Y. Zhou, K. Kanoda, and T.-K. Ng, Quantum spin liquid states, *Rev. Mod. Phys.* 89, 025003 (2017)
5. Y. Kohama, H. Ishikawa, A. Matsuo, K. Kindo, N. Shannon, and Z. Hiroi, Possible observation of quantum spin-nematic phase in a frustrated magnet, *Proc. Nat. Acad. Sci.* 116, 10686 (2019)
6. A. Kitaev, Anyons in an exactly solved model and beyond, *Ann. Phys.* 321, 2 (2006)
7. D. Bergman, J. Alicea, E. Gull, S. Trebst, and L. Balents, Order-by-disorder and spiral spin-liquid in frustrated diamond-lattice antiferromagnets, *Nature Phys.* 3, 487 (2007)
8. S. Lee and L. Balents, Theory of the ordered phase in A-site antiferromagnetic spinels, *Phys. Rev. B* 78, 144417 (2008)
9. L. Seabra, P. Sindzingre, T. Momoi, and N. Shannon, Novel phases in a square-lattice frustrated ferromagnet: 13-magnetization plateau, helicoidal spin liquid, and vortex crystal, *Phys. Rev. B* 93, 085132 (2016)
10. T. Shimokawa, T. Okubo, and H. Kawamura, Multiple-q states of the J_1 - J_2 classical honeycomb-lattice Heisenberg antiferromagnet under a magnetic field, *Phys. Rev. B* 100, 224404 (2019)
11. S. Gao, O. Zaharko, V. Tsurkan, Y. Su, J. S. White, G. S. Tucker, B. Roessli, F. Bourdarot, R. Sibille, D. Chernyshov, T. Fennell, A. Loidl, and C. Rüegg, Spiral spin-liquid and the emergence of a vortex-like state in MnSc_2S_4 , *Nature Phys.* 13, 157 (2016)

12. T. Shimokawa and H. Kawamura, Ripple state in the frustrated honeycomb-lattice antiferromagnet, *Phys. Rev. Lett.* 123, 057202 (2019)
13. S. Gao, H. D. Rosales, F. A. Gomez Albarracn, V. Tsurkan, G. Kaur, T. Fennell, P. Steens, M. Boehm, P. Cermak, A. Schneidewind, et al., Fractional antiferromagnetic skyrmion lattice induced by anisotropic couplings, *Nature* 586, 37 (2020)
14. X. Bai, J. A. M. Paddison, E. Kapit, S. M. Koohpayeh, J.-J. Wen, S. E. Dutton, A. T. Savici, A. I. Kolesnikov, G. E. Granroth, C. L. Broholm, J. T. Chalker, and M. Mourigal, Magnetic excitations of the classical spin liquid MgCr_2O_4 , *Phys. Rev. Lett.* 122, 097201 (2019)
15. M. M. Bordelon, C. Liu, L. Posthuma, E. Kenney, M. J. Graf, N. P. Butch, A. Banerjee, S. Calder, L. Balents, and S. D. Wilson, Frustrated Heisenberg J_1 - J_2 model within the stretched diamond lattice of LiYbO_2 , arXiv: 2009.04043 (2020)
16. S. Biswas and K. Damle, Semiclassical theory for liquidlike behavior of the frustrated magnet $\text{Ca}_{10}\text{Cr}_7\text{O}_{28}$, *Phys. Rev. B* 97, 115102 (2018)
17. R. Pohle, H. Yan, and N. Shannon, How many spin liquids are there in $\text{Ca}_{10}\text{Cr}_7\text{O}_{28}$? arXiv: 1711.03778 (2017)
18. A. Mulder, R. Ganesh, L. Capriotti, and A. Paramekanti, Spiral order by disorder and lattice nematic order in a frustrated heisenberg antiferromagnet on the honeycomb lattice, *Phys. Rev. B* 81, 214419 (2010)
19. P. Balla, Y. Iqbal, and K. Penc, Ane lattice construction of spiral surfaces in frustrated Heisenberg models, *Phys. Rev. B* 100, 140402 (2019)
20. P. Balla, Y. Iqbal, and K. Penc, Degenerate manifolds, helimagnets, and multi- Q chiral phases in the classical Heisenberg antiferromagnet on the face-centered-cubic lattice, *Phys. Rev. Res.* 2, 043278 (2020)
21. N. Niggemann, M. Hering, and J. Reuther, Classical spiral spin liquids as a possible route to quantum spin liquids, *J. Phys.: Condens. Matter* 32, 024001 (2019)
22. Z. Nussinov, Commensurate and incommensurate $\text{o}(\text{n})$ spin systems: Novel even-odd effects, a generalized mermin-wagner-coleman theorem, and ground states, arXiv: 0105253 (2004)
23. J. Attig and S. Trebst, Classical spin spirals in frustrated magnets from free-fermion band topology, *Phys. Rev. B* 96, 085145 (2017)
24. J. Villain, R. Bidaux, J.-P. Carton, and R. Conte, Order as an effect of disorder, *Journal de Physique* 41, 1263 (1980)
25. C. L. Henley, Ordering due to disorder in a frustrated vector antiferromagnet, *Phys. Rev. Lett.* 62, 2056 (1989)
26. J. N. Reimers and A. J. Berlinsky, Order by disorder in the classical Heisenberg Kagomé antiferromagnet, *Phys. Rev. B* 48, 9539 (1993)
27. K. Hukushima and K. Nemoto, Exchange Monte Carlo method and application to spin glass simulations, *J. Phys. Soc. Japan* 65, 1604 (1996)
28. N. Tristan, J. Hemberger, A. Krimmel, H.-A. Krug von Nidda, V. Tsurkan, and A. Loidl, Geometric frustration in the cubic spinels $M\text{Al}_2\text{O}_4$ ($M = \text{Co}, \text{Fe}, \text{and Mn}$), *Phys. Rev. B* 72, 174404 (2005)
29. T. Suzuki, H. Nagai, M. Nohara, and H. Takagi, Melting of antiferromagnetic ordering in spinel oxide CoAl_2O_4 , *J. Phys.: Condens. Matter* 19, 145265 (2007)
30. V. Fritsch, J. Hemberger, N. Büttgen, E.-W. Scheidt, H.-A. Krug von Nidda, A. Loidl, and V. Tsurkan, Spin and orbital frustration in MnSc_2S_4 and FeSc_2S_4 , *Phys. Rev. Lett.* 92, 116401 (2004)
31. O. Zaharko, N. B. Christensen, A. Cervellino, V. Tsurkan, A. Maljuk, U. Stuhr, C. Niedermayer, F. Yokaichiya, D. N. Argyriou, M. Boehm, and A. Loidl, Spin liquid in a single crystal of the frustrated diamond lattice antiferromagnet CoAl_2O_4 , *Phys. Rev. B* 84, 094403 (2011)
32. Y. Iqbal, T. Müller, H. O. Jeschke, R. Thomale, and J. Reuther, Stability of the spiral spin liquid in MnSc_2S_4 , *Phys. Rev. B* 98, 064427 (2018)
33. J. R. Chamorro, L. Ge, J. Flynn, M. A. Subramanian, M. Mourigal, and T. M. McQueen, Frustrated spin one on a diamond lattice in NiRh_2O_4 , *Phys. Rev. Mater.* 2, 034404 (2018)
34. L. Ge, J. Flynn, J. A. M. Paddison, M. B. Stone, S. Calder, M. A. Subramanian, A. P. Ramirez, and M. Mourigal, Spin order and dynamics in the diamond-lattice Heisenberg antiferromagnets CuRh_2O_4 and CoRh_2O_4 , *Phys. Rev. B* 96, 064413 (2017)
35. G. Chen, Quantum paramagnet and frustrated quantum criticality in a spin-one diamond lattice antiferromagnet, *Phys. Rev. B* 96, 020412 (2017)
36. F. L. Buessen, M. Hering, J. Reuther, and S. Trebst, Quantum spin liquids in frustrated spin-1 diamond antiferromagnets, *Phys. Rev. Lett.* 120, 057201 (2018)
37. F.-Y. Li and G. Chen, Spin-orbital entanglement in d^8 Mott insulators: Possible excitonic magnetism in diamond lattice antiferromagnets, *Phys. Rev. B* 100, 045103 (2019)
38. S. Das, D. Nafday, T. Saha-Dasgupta, and A. Paramekanti, NiRh_2O_4 : A spin-orbit entangled diamond-lattice paramagnet, *Phys. Rev. B* 100, 140408 (2019)
39. S. A. Nikolaev, I. V. Solovyev, A. N. Ignatenko, V. Y. Irkhin, and S. V. Streltsov, Realization of the anisotropic compass model on the diamond lattice of Cu^{2+} in CuAl_2O_4 , *Phys. Rev. B* 98, 201106 (2018)
40. X.-P. Yao, C.-J. Huang, C. Liu, F.-Y. Li, and G. Chen, The effects of spin-orbit coupling in diamond lattice magnets: A study of heisenberg-compass model on a diamond lattice (2020) (in preparation)
41. J. G. Cheng, G. Li, L. Balicas, J. S. Zhou, J. B. Goodenough, C. Xu, and H. D. Zhou, High-pressure sequence of $\text{Ba}_3\text{NiSb}_2\text{O}_9$ structural phases: New $S = 1$ quantum spin liquids based on Ni^{2+} , *Phys. Rev. Lett.* 107, 197204 (2011)
42. G. Chen, M. Hermele, and L. Radzihovsky, Frustrated quantum critical theory of putative spin-liquid phenomenology in $6\text{H-B-Ba}_3\text{NiSb}_2\text{O}_9$, *Phys. Rev. Lett.* 109, 016402 (2012)
43. S. Okumura, H. Kawamura, T. Okubo, and Y. Motome, Novel spin-liquid states in the frustrated Heisenberg antiferromagnet on the honeycomb lattice, *J. Phys. Soc. Japan* 79, 114705 (2010)

44. M. Matsuda, M. Azuma, M. Tokunaga, Y. Shimakawa, and N. Kumada, Disordered ground state and magnetic field-induced long-range order in an $S = 3/2$ antiferromagnetic honeycomb lattice compound $\text{Bi}_3\text{Mn}_4\text{O}_{12}(\text{NO}_3)$, *Phys. Rev. Lett.* 105, 187201 (2010)
45. T. A. Sedrakyán, L. I. Glazman, and A. Kamenev, Spontaneous formation of a nonuniform chiral spin liquid in a moat-band lattice, *Phys. Rev. Lett.* 114, 037203 (2015)
46. S. Jiang, L. Zou, and W. Ku, Non-Fermi-liquid scattering against an emergent Bose liquid: Manifestations in the kink and other exotic quasiparticle behavior in the normal-state cuprate superconductors, *Phys. Rev. B* 99, 104507 (2019)
47. Z. Wang, C. Navarrete-Benlloch, and Z. Cai, Pattern formation and exotic order in driven-dissipative Bose-Hubbard systems, *Phys. Rev. Lett.* 125, 115301 (2020)
48. J.-S. Bernier, M. J. Lawler, and Y. B. Kim, Quantum order by disorder in frustrated diamond lattice antiferromagnets, *Phys. Rev. Lett.* 101, 047201 (2008)